



Article

Structure of Cu, Ni, and CuNi Bimetallic Small Clusters Incorporated in g-C₃N₄: A DFT Study

Agnieszka Drzewiecka-Matuszek, Priti Sharma and Dorota Rutkowska-Zbik *

Jerzy Haber Institute of Catalysis and Surface Chemistry, Polish Academy of Sciences, ul. Niezapominajek 8, 30-239 Krakow, Poland; agnieszka.drzewiecka-matuszek@ikifp.edu.pl (A.D.-M.); priti.sharma@ikifp.edu.pl (P.S.) * Correspondence: dorota.rutkowska-zbik@ikifp.edu.pl; Tel.: +48-12-6395160

Abstract

Graphitic carbon nitride is recognized as a very promising support structure to anchor single atoms and small, sub-nanometric metal clusters, with vast applications in catalysis. In the current manuscript, we aim to study the geometry and electronic structures of the small, sub-nanometric monometallic (copper or nickel) and bimetallic (copper–nickel) clusters anchored to the graphitic carbon nitride. Our Density Functional Theory (DFT) study reveals that Cu and Ni, when in the form of isolated single atoms, lie in the plane of the support. Once the atoms agglomerate and form small clusters, they tend to bind above the carbon nitride (C_3N_4) plane. The nickel atoms form shorter bonds with the support than the copper atoms do, which is reflected by the binding energies. Atoms directly bound to the support become oxidized, forming electrophilic sites at the surface. The computed negative metal–support binding energies mean that the investigated Cu/Ni- C_3N_4 composites are stable, and the metal species will not easily leach from the support.

Keywords: copper; nickel; graphitic carbon nitride; single-atom catalyst; Density Functional Theory (DFT)



Academic Editor: Jinxing Chen

Received: 31 July 2025 Revised: 21 August 2025 Accepted: 22 August 2025 Published: 6 September 2025

Citation: Drzewiecka-Matuszek, A.; Sharma, P.; Rutkowska-Zbik, D. Structure of Cu, Ni, and CuNi Bimetallic Small Clusters Incorporated in g-C₃N₄: A DFT Study. *Catalysts* **2025**, *15*, 861. https://doi.org/ 10.3390/catal15090861

Copyright: © 2025 by the authors. Licensee MDPI, Basel, Switzerland. This article is an open access article distributed under the terms and conditions of the Creative Commons Attribution (CC BY) license (https://creativecommons.org/licenses/by/4.0/).

1. Introduction

In recent years, there has been increasing interest in two-dimensional (2D) structures as catalysts and supports for catalytic materials, with graphene, MXenes (transition-metal carbides and nitrides), boron nitride (BN), and carbon nitride (C_3N_4) being the most often studied [1–6]. Their tunable chemistry combined with unique surface properties makes them promising for use in various applications, in particular for electro- and photocatalytic processes involving transformations of small molecules such as CO_2 reduction, water splitting to hydrogen and/or oxygen, and direct ammonia synthesis from dinitrogen, to name only a few. An important field of research is their use as supports for isolated atom sites or small, sub-nanometric metal clusters.

Catalysis by single-atom catalysts (SACs) is an emerging and very active topic, as these materials have been found to have several advantages over typical materials composed of the metal phase deposited on the support [7–11]. There are claims that not only single atoms but also small, sub-nanometric metallic clusters can be formed and anchored to different supports to contribute to the catalytic activity of these materials [12–17].

In the current manuscript, we aim to study the structural properties of graphitic carbon nitride $(g-C_3N_4)$ as a host material that can accommodate small clusters of transition metals. Here, we focus our attention on copper and nickel as both belong to Earth-abundant, nonnoble elements with vast applications in catalysis for the valorization of carbon dioxide,

Catalysts 2025, 15, 861 2 of 17

hydrogen evolution, water splitting, biomass upgrading, etc. [18]. In particular, both metals are also incorporated in g- C_3N_4 to form a so-called "single-atom catalyst" (SAC), whose activity is generally believed to be higher than that of typically supported Cu/Ni nanoparticles [19]. Our research questions include whether the single copper and nickel atoms are stable when incorporated in g- C_3N_4 , what structures they have, and whether they can form small clusters anchored to the support. Furthermore, we also aim to explore the possibility of g- C_3N_4 to accommodate very small, bimetallic CuNi clusters of various Cu:Ni ratios.

In the literature, theoretical studies exist on single Cu and Ni atoms anchored to the graphitic carbon nitride, usually forming bonds with the nitrogen atoms at the edges of the cavity in between the heptazine units (the so-called M-N₄ site) [20]. Occasionally, it has been proposed that the metal site occupies the carbon vacancy site in a melamine unit, forming three bonds with the nitrogen atoms (a so-called M-N₃ site) [20]. Recently, a combined theoretical and advanced spectroscopic study proposed that single-nickel sites are located at the edges of various sheets of carbon nitride, which offers a favorable coordination environment for Ni (possibility to form four equivalent Ni-N bonds) [21]. There are also some reports on small, sub-nanometric clusters anchored to g-C₃N₄. They refer mostly to tetrahedral M₄ units, which span most of the fourth period of the periodic table [12,13]. Pairs have been considered for iron [15], scandium, titanium, vanadium, and nickel [22], while triples have been investigated for ruthenium [14] and copper [23]. A systematic study on the possibility of the carbon nitride by Ti_n (n = 1-4) moieties was published by Zhang et al. [24], who considered binding titanium atoms above the melamine units. To our knowledge, there is a lack of research on the mixed CuNi systems anchored on g-C₃N₄, despite the proposed activity of such bimetallic sites in, e.g., CO₂ hydrogenation [25].

2. Results and Discussion

The present theoretical study involved the basic building unit of the g- C_3N_4 structure comprising three heptazine "triangles" with a cavity in between, which can accommodate molecular ensembles (see Figure 1). The binding of up to four metal atoms (Cu, Ni, and a combination thereof) with the g- C_3N_4 support was examined.

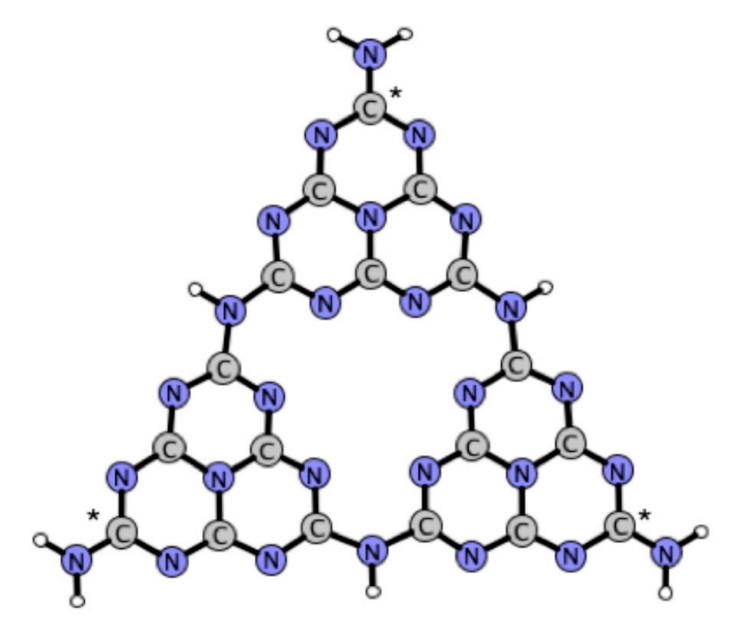


Figure 1. Theoretical model of the g- C_3N_4 fragment adopted in the current study. Asterisks (*) denote carbon atoms frozen during the geometry optimization procedure. Atom color coding: C—gray; N—blue; H—white.

Catalysts **2025**, 15, 861 3 of 17

2.1. Cu_n - C_3N_4 (n = 1-4) Structures

Figure 2 presents the structures of the optimized Cu_n - C_3N_4 clusters (n = 1-4).

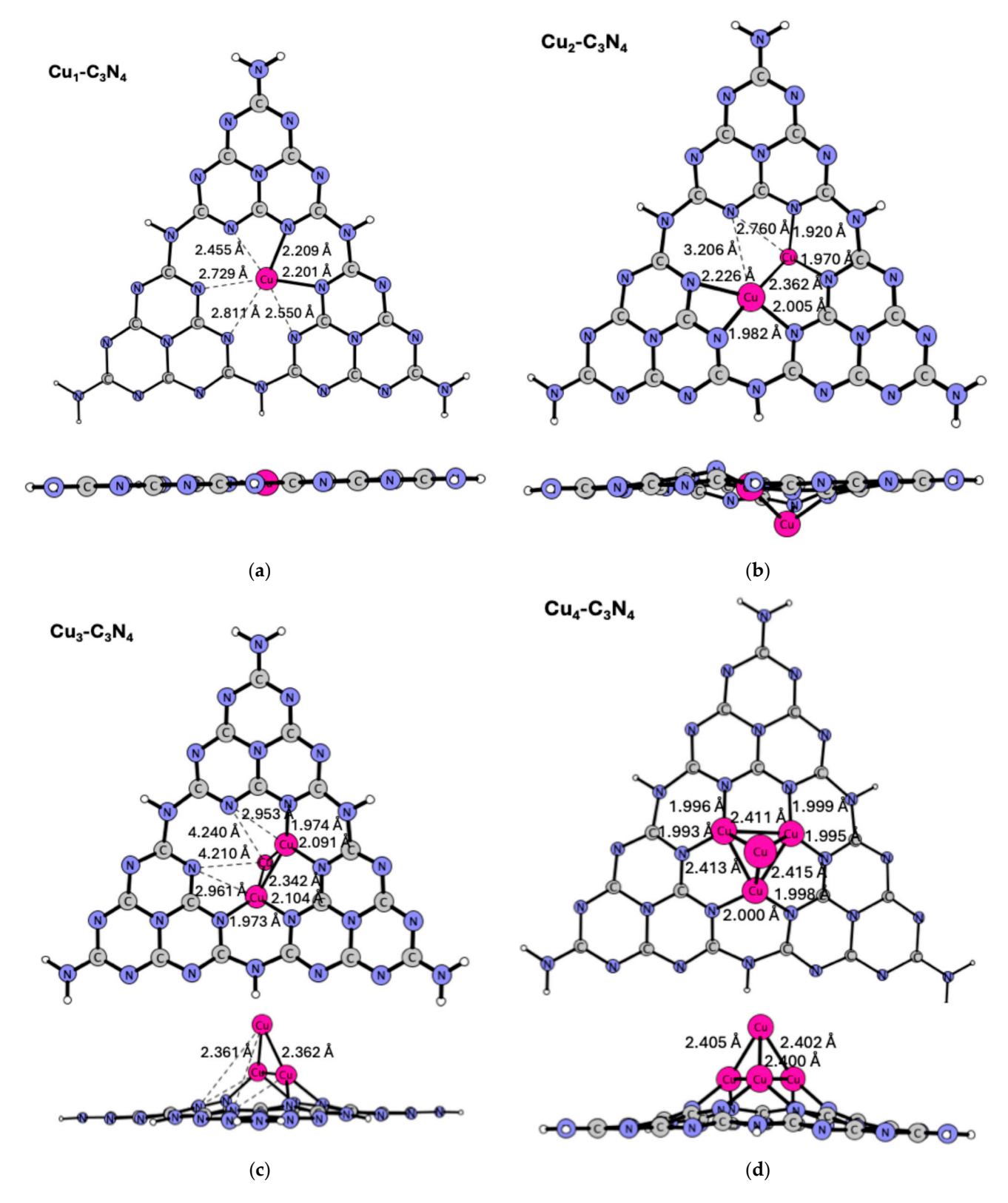


Figure 2. DFT:PBE/def2-TZVP structures of (a) Cu-C $_3$ N $_4$; (b) Cu $_2$ -C $_3$ N $_4$; (c) Cu $_3$ -C $_3$ N $_4$; and (d) Cu $_4$ -C $_3$ N $_4$. The most characteristic bond lengths are given in Ångstroms. Atom color coding: Cu—pink; C—gray; N—blue; H—white.

Catalysts **2025**, 15, 861 4 of 17

When a single copper atom was inserted into the carbon nitride, it was located in the plane of the g-C₃N₄ support, forming two shorter bonds (2.201 Å and 2.209 Å) and four longer bonds (2.455 Å, 2.550 Å, 2.729 Å, and 2.811 Å) with the nitrogen atoms. Such a coordination is often referred to as Cu-N₄ [20]. The bond length values are comparable to the Density Functional Theory (DFT) data reported previously for the single Cu atom anchored to g-C₃N₄; Yang et al. claimed two shorter bonds of 2.16 Å and 2.18 Å and two longer bonds of 2.28 Å and 2.38 Å [20], while Zhao et al. reported two bonds of 2.11 Å [26]. The structure has one unpaired electron. The natural population analysis (NPA) reveals that the copper atom is oxidized when bound to the support (the NPA charge on Cu is equal to 0.82). This finding agrees with the earlier reports on Cu-C₃N₄ [20,26].

When the second copper atom was added, the g- C_3N_4 model started to ruffle. The second copper is located at a distance of 2.362 Å from the first one. The bonds between the Cu and N atoms became shorter than in the case of the single-copper structure. The closer nitrogen atoms are located at 1.920 Å, 1.970 Å, 1.982 Å, and 2.005 Å, while the further ones are located at 2.226 Å, 2.760 Å, and 3.206 Å. These bond lengths correspond to the values resulting from the Extended X-ray Absorption Fine Structure (EXAFS) measurements for the SAC-type Cu- C_3N_4 , where several peaks for the Cu-N distances (at ca. 1.5 Å, 2.0 Å, 2.5 Å, and 3.5 Å) were visible [20]. Therefore, one can put forward a hypothesis that the material might contain a small admixture of the Cu₂ sites as well. The structure is characterized by two unpaired electrons. The NPA charges of copper, being equal to 0.80 and 0.76, indicate the oxidation of the copper atoms and their cationic character.

When three copper atoms were anchored onto g- C_3N_4 , none of them stayed in the plane. They started to form a 3D-like cluster above the support, with two Cu atoms bound to the nitrogen atoms (bond lengths are equal to 1.973 Å, 1.974 Å, 2.091 Å, and 2.104 Å), and the third one above them (the Cu-Cu bond distances are equal to 2.342 Å, 2.361 Å, and 2362 Å). There is one unpaired electron in the system. The natural population charges indicate that both Cu atoms, which are directly bound to g- C_3N_4 , are mildly oxidized (with charges equal to 0.52 and 0.53), while the "top" copper atom is slightly reduced (with a charge equal to -0.12).

In the structure with four Cu atoms, a Cu₄ tetrahedron is located above the center of the cavity in g-C₃N₄. During the investigation, we also found a structure in which two copper atoms are located above the C₃N₄ plane, and two other atoms are located below the plane, but the structure had a higher total energy by 2.77 eV than the one reported here (see Figure S1 in the Supplementary Materials). In the minimum energy structure, the three lower copper atoms form bonds of ca. 2.0 Å with the support. The Cu-Cu distances are in the range of 2.400–2.415 Å; the longer ones are found between the atoms forming the base for the small cluster, while the shorter ones are found for atoms connecting the base with its top. They are comparable with the Cu-Cu bond lengths in the metallic copper (2.53 Å) [27], as well as in the 2D copper monolayer (2.41 Å) [28]. The multiplicity of the resulting structure is three. Interestingly, the copper atoms that form the base of the tetrahedron are mildly oxidized (their charges amount to 0.55, 0.56, and 0.56), whereas the one at the top is almost neutral (0.02).

Previous studies on g- C_3N_4 indicated that the modification of the material via the introduction of $C\equiv N$, C=O, and O-H substituents influenced its HOMO-LUMO gap [29]. Here, we were interested in whether a similar effect could be observed in the case of the metal cluster incorporation into the structure (see Figure 3 for a schematic representation of the electronic structure of the hybrids). The HOMO-LUMO energy difference in the model of the g- C_3N_4 material equals 2.37 eV, which is in reasonable agreement with [29]. The valence band edge changes depending on the number of copper atoms introduced to the system, but the conduction band edge is practically not affected. As a result, the gap is

Catalysts **2025**, 15, 861 5 of 17

modified, which can lead to variation in the photocatalytic properties. Once copper was introduced, additional electronic states appeared in the gap. The presence of these in-band gap states can further modify light absorbance properties and may also be responsible for a faster electron–hole recombination [30].

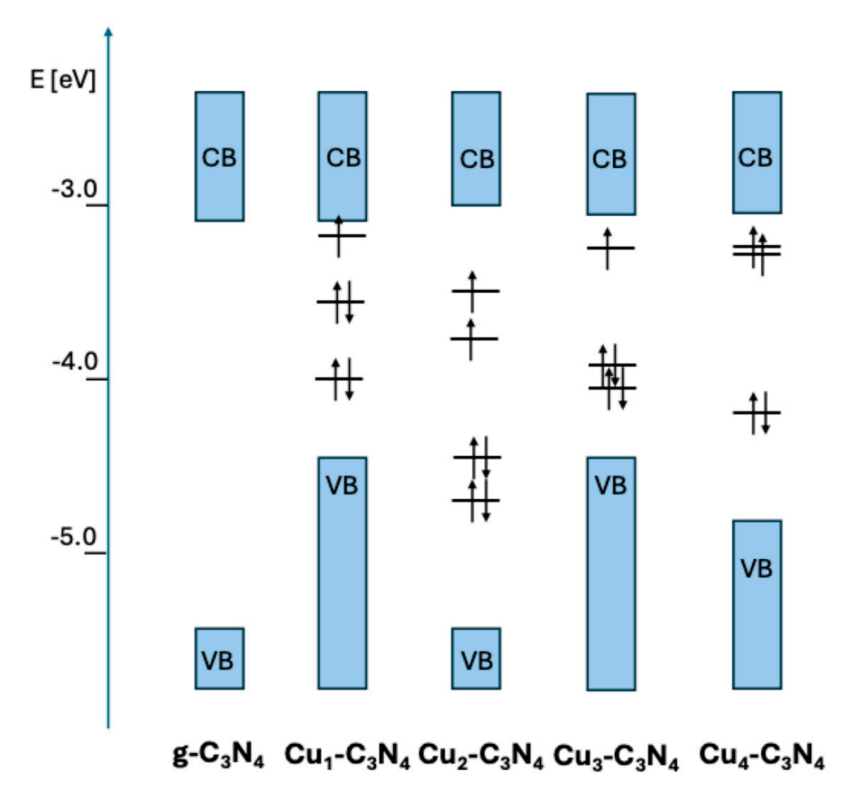


Figure 3. Schematic representation of the electronic structure of the Cu_n - C_3N_4 systems (VB—valence band; CB—conduction band). For the open-shell systems, the diagram represents alpha electrons.

Next, we calculated the energy parameters characterizing the strength of the interaction between the copper atoms and their support (see Table 1). Table 1 displays the binding energy (E_{bin}) between the metal phase and g- C_3N_4 , calculated according to Equation (1) as defined in the Materials and Methods Section; the nucleation energy ($E_{nuc\text{-}gas}$), calculated according to Equation (2) as defined therein; and the energy needed to migrate an additional metal atom from its SAC-like position to form a larger species ($E_{nuc\text{-}SAC}$), calculated according to Equation (3) ibid. Furthermore, it lists the reorganization energy of the metal cluster (E_{reor}) as defined by Equation (4).

Table 1. The energetic parameters (E_{bin} , $E_{nuc\text{-}gas}$, $E_{nuc\text{-}SAC}$, and E_{reor}) in [eV] computed for the Cu_n - C_3N_4 structures at the DFT:PBE/def2-TZVP level. For their definitions, see Equations (1)–(4) in the Materials and Methods Section.

System	E _{bin} [eV]	E _{nuc-gas} [eV]	E _{nuc-SAC} [eV]	E _{reor} [eV]
Cu ₁ -C ₃ N ₄	-2.29	-	-	-
Cu_2 - C_3N_4	-1.35	-1.14	1.15	0.02
Cu_3 - C_3N_4	-3.18	-3.13	-0.84	0.04
Cu_4 - C_3N_4	-3.64	-3.01	-0.72	1.09

It is seen that in all investigated systems, the copper moiety binds favorably to the support; all calculated binding energies are negative. The strength of the binding of the Cu_2 cluster is the smallest, while the strength of the binding of the tetrahedral Cu_4 is the largest.

Catalysts **2025**, 15, 861 6 of 17

Next, it is seen that the copper clusters tend to grow larger, in particular when the additional atom is introduced from the gas phase (see the reported $E_{\text{nuc-gas}}$ energy values). Only one $E_{\text{nuc-SAC}}$ energy parameter is positive, meaning that the aggregation of two copper atoms, which were previously anchored to $g\text{-}C_3N_4$ as the single atom sites, is not thermodynamically privileged. This results from the fact that the binding of the single Cu atom is more energetically beneficial than the binding of the pair of Cu atoms (see the E_{bin} values for $Cu_1\text{-}C_3N_4$ and $Cu_2\text{-}C_3N_4$). It should be noted here, however, that in the current study, the reaction pathway of the metal atom moving from one anchor site to the other has not been considered; hence, we are not able to comment on the kinetics of such a migration.

Finally, the analysis of the metal cluster reorganization energies revealed that the geometries of the Cu₂ and Cu₃ clusters are almost identical regardless of the environment, i.e., if they are free, in the gas phase, or anchored to g-C₃N₄. The high reorganization energy of the Cu₄ cluster can be justified by the fact that in the gas phase, the Cu₄ cluster prefers a planar geometry, which follows from our calculations and previous studies found in the literature [31].

2.2. Structures of Ni_n - C_3N_4 (n = 1-4)

Figure 4 presents the resulting geometries of the Ni_n - C_3N_4 structures (n = 1-4).

The single nickel atom stays in the plane of the g- C_3N_4 , with Ni-N bond lengths of 1.920 Å and 1.927 Å. The remaining Ni-N distances are longer and equal to 2.510 Å, 2.609 Å, 3.110 Å, and 3.170 Å. The comparison with Cu- C_3N_4 reveals that the nickel atom tends to bind closer than the copper atom to the heptazine fragment of the support. The total multiplicity of the system is three, meaning that two unpaired electrons are present. The nickel atom is positively charged (the NPA charge equals 0.78), which is in agreement with the FT-IR studies indicating the cationic character of the single-nickel site in g- C_3N_4 [21].

In the case of the Ni_2 - C_3N_4 , both nickel atoms have a very similar coordination environment. Each of them forms three bonds with nitrogen atoms of the support (two shorter bonds of 1.871 Å, 1.872 Å, 1.874 Å, and 1.880 Å, and one longer bond of 2.077 Å and 2.094 Å). Therefore, the resulting structure is more symmetric than Cu_2 - C_3N_4 . Here, the Ni atoms point above the support plane in opposite directions, and the local structure is not as ruffled as it was found in the copper system. The Ni-Ni distance amounts to 2.199 Å. Both nickel atoms are oxidized (the NPA charges are the same for both sites and equal to 0.57).

In the structure with three nickel atoms, one nickel is lying in the plane of the support, while the remaining two are symmetrically pointing up and down (see Figure 4c). The one in the plane forms bonds of 1.873~Å, 1.950~Å, and 2.310~Å with the support nitrogen atoms. The two others are located at distances of 1.973~Å, 1.978~Å, 2.010~Å, and 2.012~Å from the closest nitrogen atoms and 2.345~Å from the Ni atom that is located in the plane. The Ni-Ni bond is 2.413~Å long. The geometry of the support is flat. There are four unpaired electrons in the system, with slightly positively charged nickel atoms (their charges are equal to 0.54, 0.55, and 0.56).

Finally, the structure in which the Ni₄ cluster interacts with g-C₃N₄ is very similar to Cu₄-C₃N₄. Four nickel atoms form the tetrahedral unit above the cavity. The Ni-N bonds are in the range of 1.883 Å–1.980 Å, and the Ni-Ni bonds are 2.275 Å–2.279 Å long for the Ni atoms lying in the base of the tetrahedron and 2.355 Å–2.361 Å when formed between the top Ni atom and the remaining three atoms. These are somewhat shorter than the Ni-Ni distances in the metallic nickel, where each Ni atom forms six shorter (2.45 Å) and six longer (2.48 Å) bonds with its neighbors [27]. The resulting structure has a triplet multiplicity. The three base nickel atoms have 0.40, 0.41, and 0.41 charges, while the one on top of them is practically neutral (its charge amounts to -0.02).

Catalysts **2025**, 15, 861 7 of 17

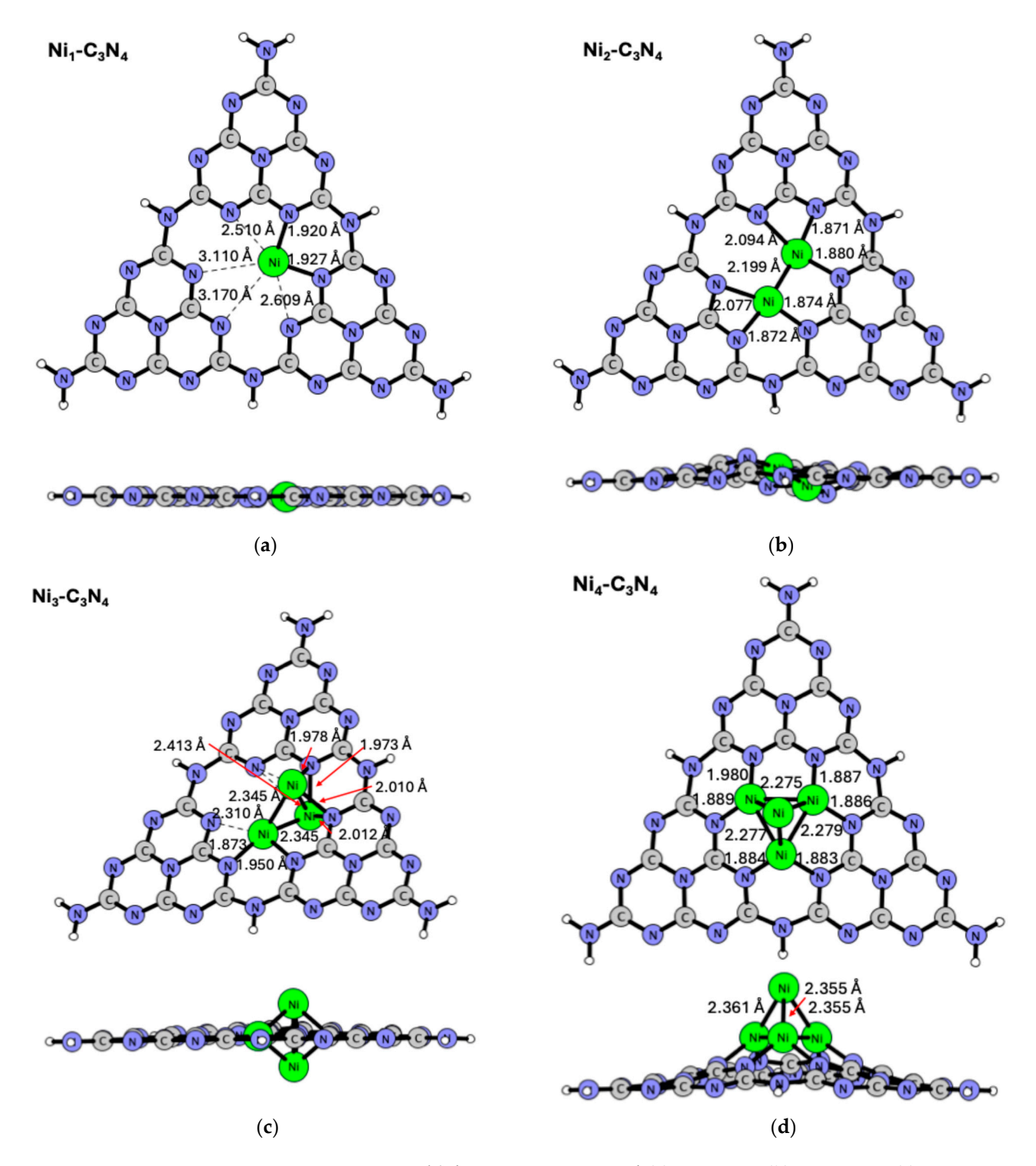


Figure 4. DFT:PBE/def2-TZVP structures of (a) Ni-C $_3$ N $_4$; (b) Ni $_2$ -C $_3$ N $_4$; (c) Ni $_3$ -C $_3$ N $_4$; and (d) Ni $_4$ -C $_3$ N $_4$. The most characteristic bond lengths are given in Ångstroms. Atom color coding: Ni—green; C—gray; N—blue; H—white.

Similarly, as found for copper-based systems, the nickel incorporation into g- C_3N_4 results in the HOMO-LUMO band gap narrowing and the appearance of the electronic in-band states (see Figure 5).

Catalysts **2025**, 15, 861 8 of 17

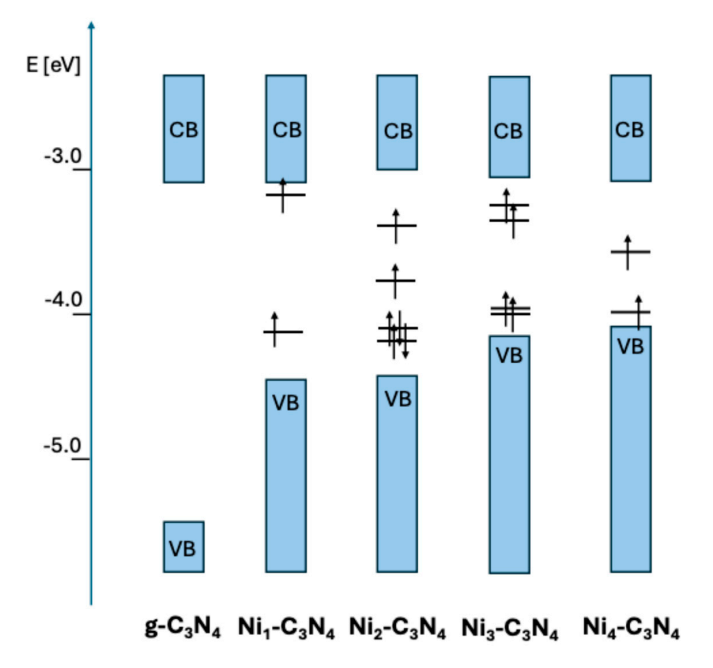


Figure 5. Schematic representation of the electronic structure of the Ni_n - C_3N_4 systems (VB—valence band; CB—conduction band). For the open-shell systems, the diagram represents alpha electrons.

Table 2 displays energetic parameters characterizing the strength of the metal–support interaction as well as the tendency of the nickel atoms to form larger clusters at the g- C_3N_4 surface.

Table 2. The energetic parameters (E_{bin} , $E_{nuc\text{-}gas}$, $E_{nuc\text{-}SAC}$, and E_{reor}) in [eV] computed for the Ni_n-C₃N₄ structures at the DFT:PBE/def2-TZVP level. For their definitions, see Equations (1)–(4) in the Materials and Methods Section.

System	E _{bin} [eV]	E _{nuc-gas} [eV]	E _{nuc-SAC} [eV]	E _{reor} [eV]
Ni ₁ -C ₃ N ₄	-4.86	-	-	-
Ni_2 - C_3N_4	-3.71	-4.43	0.43	0.00
Ni_3 - C_3N_4	-2.41	-2.72	2.14	0.72
Ni ₄ -C ₃ N ₄	-5.13	-7.15	-2.29	0.07

The examination of the nickel clusters' binding energies shows that the nickel species binds more strongly to the g- C_3N_4 surface than copper does. This finding corroborates the idea that Ni-N bonds are generally shorter than Cu-N bonds, which cannot be simply explained by the differences in the atomic radii of the studied elements (1.28 Å for Cu and 1.24 Å for Ni). Only Cu₃ binds more strongly to carbon nitride than Ni₃ does, which might result from the differences in the geometries between the two structures.

All $E_{nuc\text{-}gas}$ energies are negative, indicating that the nickel clusters tend to enlarge when the additional Ni atom comes from the gas phase. Conversely, the $E_{nuc\text{-}SAC}$ energies are positive in the case of $Ni_2\text{-}C_3N_4$ and $Ni_3\text{-}C_3N_4$, meaning that the growth of the Ni_2 and Ni_3 clusters at the expense of the Ni atom previously incorporated into g- C_3N_4 is unfavorable. This is a consequence of the very strong binding energy of the single nickel atom to the studied support.

The analysis of the cluster reorganization energies reveals that the Ni $_3$ cluster is the most distorted compared to its geometry in the gas phase, which manifests in an E $_{\rm reor}$ value equal to 0.72 eV. In the planar gas-phase Ni $_3$ cluster, the Ni-Ni bonds are equal to 2.238 Å, 2.238 Å, and 2.247 Å, which is much shorter than in Ni $_3$ -C $_3$ N $_4$. These Ni-Ni bond lengths are comparable to the results of the other theoretical studies, which can be found in

Catalysts 2025, 15, 861 9 of 17

the literature [32,33]. It is worth mentioning that, unlike in the case of copper, Ni_4 prefers the tetrahedral geometry in the gas phase, which is reflected in the minor E_{reor} value, as indicated by previous studies (see [33] and the references therein).

2.3. Cu_nNi_m - C_3N_4 (n = 1-3; m = 1-3) Structures

Various combinations of copper and nickel atoms were considered (see Figure 6 for the structures described below).

In CuNi- C_3N_4 , the nickel atom stays practically in the plane of the cavity, while the copper atom is pulled above it. Accordingly, nickel forms shorter bonds with nitrogen (1.903 Å, 1.907 Å, and 2.122 Å) than copper does (1.948 Å, 2.048 Å, and 2.572 Å). Both atoms are located at a distance of 2.306 Å from each other. The structure has only one unpaired electron. Both metal atoms are oxidized (the charge on Cu amounts to 0.79 and the charge on Ni amounts to 0.57).

In both structures with three metal atoms, namely Cu₂Ni-C₃N₄ and CuNi₂-C₃N₄, the metal clusters form a triangle-like moiety, which is located above the g- C_3N_4 plane, like in Cu₃-C₃N₄. In Cu₂Ni-C₃N₄, the base of the triangle is formed by the nickel and the copper atoms (set apart by 2.321 Å), which are bound to the nitrogen atoms at distances of 1.896 Å and 1.945 Å (Ni-N) and 1.997 Å and 2.067 Å (Cu-N). The distance between the copper atom on top and the nickel atom amounts to 2.389 Å. The Cu-Cu bond length is equal to 2.358 Å. In this triplet structure, the atoms that are directly bound to the support have positive charges (Ni: 0.44; Cu: 0.54), while the Cu on top is slightly negatively charged (its charge amounts to -0.13). During our theoretical studies, we also found two other structures with the Cu₂Ni cluster anchored to g-C₃N₄, but both of them are characterized by higher total energies than the one described above (see Figure S2 in the Supplementary Materials). The first one has the nickel atom located almost in the plane of C_3N_4 , with one of the copper atoms being slightly above, and the third one being above both metal atoms. This structure is higher in energy by 0.34 eV. The second isomeric Cu₂Ni-C₃N₄ structure has two copper atoms directly bound to g-C₃N₄ and the nickel atom above, and it is higher in energy in terms of the minimum energy structure by 0.74 eV.

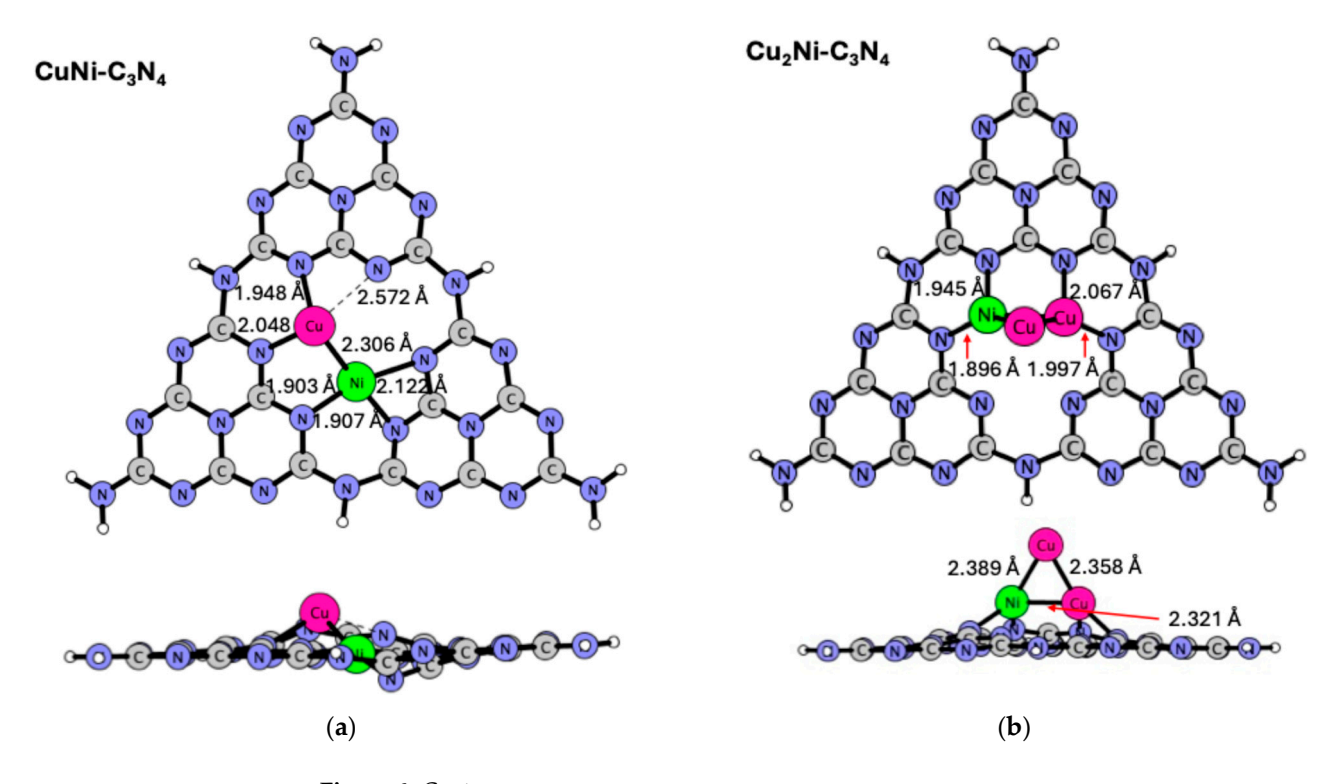


Figure 6. Cont.

Catalysts **2025**, 15, 861 10 of 17

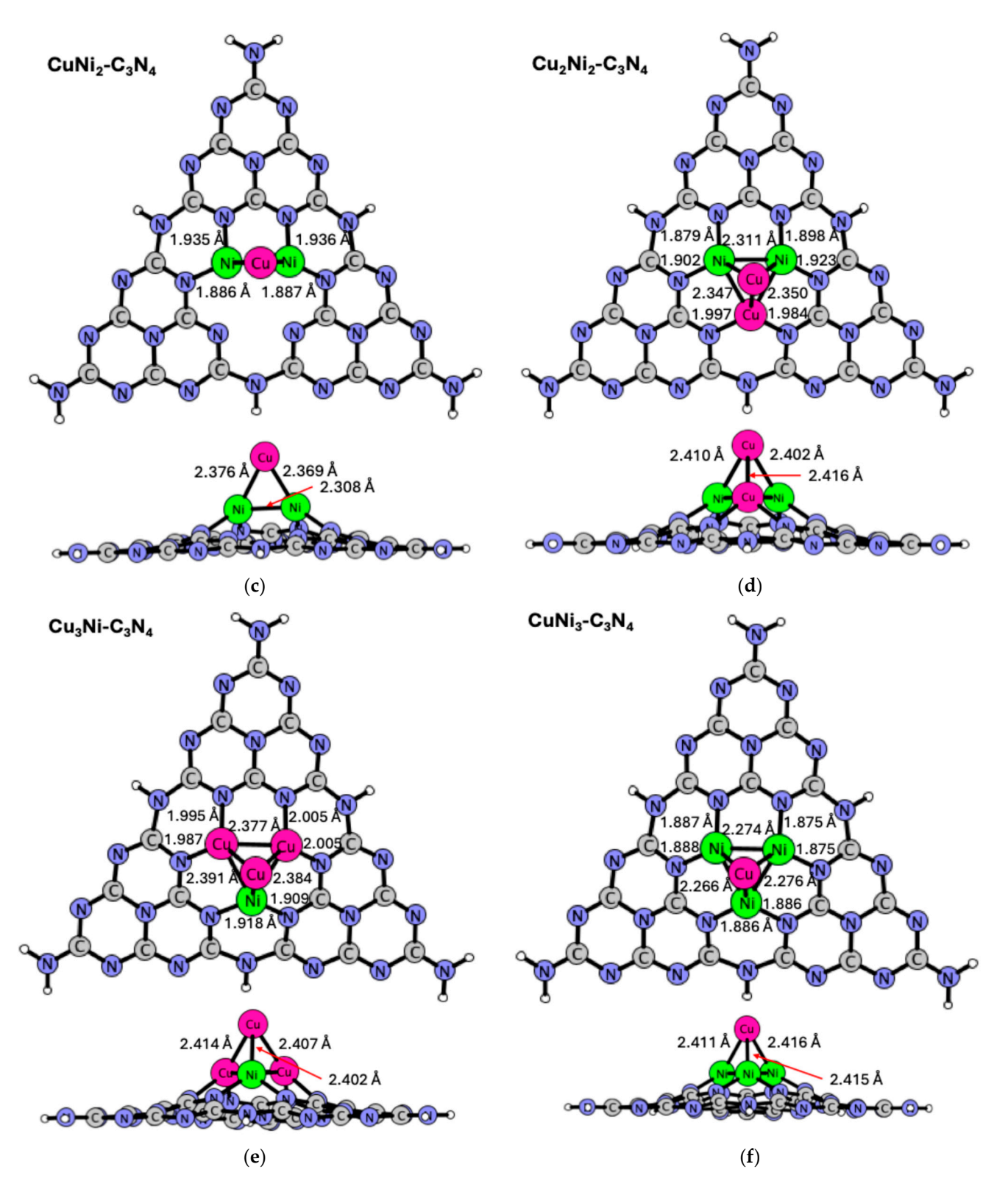


Figure 6. DFT:PBE/def2-TZVP structures of (a) CuNi- C_3N_4 ; (b) Cu₂Ni- C_3N_4 ; (c) CuNi₂- C_3N_4 ; (d) Cu₂Ni₂- C_3N_4 ; (e) Cu₃Ni- C_3N_4 ; and (f) CuNi₃- C_3N_4 . The most characteristic bond lengths are given in Ångstroms. Atom color coding: Cu—pink; Ni—green; C—gray; N—blue; H—white.

In $\text{CuNi}_2\text{-}\text{C}_3\text{N}_4$, both nickel atoms form the base of the triangle with Ni-N bonds of 1.886 Å, 1.887 Å, 1.935 Å, and 1.936 Å, and a Ni-Ni distance of 2.308 Å. The Cu-Ni bonds are equal to 2.376 Å and 2.369 Å. Spin multiplicity is equal to two. Both nickel atoms have practically the same charges (0.50 and 0.51), while copper bears a small negative charge

Catalysts **2025**, 15, 861

(-0.11). The alternative structure, in which the base of the metal triangle is composed of one nickel and one copper atom, has a total energy higher by 0.63 eV than the previously described one. Figure S3 depicts its geometry.

Finally, all bimetallic structures having four atoms have a similar structure. The metals form a tetrahedral moiety, which is bound above the g-C₃N₄ cavity, as described previously for the monometallic M_4 - C_3N_4 structures. In Cu_2Ni_2 - C_3N_4 , the base of the tetrahedron is formed by two nickel atoms and one copper atom. The structure in which nickel is on the top of the tetrahedron is characterized by an energy higher by 0.60 eV (see Figure S4). Similarly to the previous structures, in the minimum energy structure, the Ni-N bonds (1.879 Å-1.923 Å) are shorter than the Cu-N ones (1.984 Å and 1.997 Å). The copper atom on top forms two shorter bonds with two nickel atoms (2.402 Å and 2.410 Å) and a longer bond with the copper atom (2.416 Å). The nickel atoms bear a smaller charge than in the previously discussed structures (0.32 and 0.36), and the copper atom in the base of the tetrahedron is oxidized (its charge amounts to 0.58), while the copper atom on top is neutral (a charge of 0.02). In $Cu_3Ni-C_3N_4$, the nickel atom (whose NPA charge equals 0.32) is at the base of the tetrahedron and is bound to nitrogen atoms at distances of 1.909 A and 1.918 A. The copper atoms form slightly larger bonds with the support (1.987 Å-2.005 Å). The "top" copper atom forms three similar bonds with Ni (2.402 Å) and Cu (2.407 Å and 2.414 Å). While the Cu atoms in the base are oxidized (charges of 0.56 and 0.58 are calculated), the one on top of the tetrahedron is neutral (0.01). Alternatively, the second structure of this composition was found with the nickel atom located on top of the tetrahedron (see Figure S5), but its total energy is higher by 0.60 eV. In CuNi₃-C₃N₄, all nickel atoms lie in the lower layer, forming the base of the tetrahedron. The distances of the nitrogen atoms from the support are comparable and in the range between 1.875 Å and 1.888 Å. They also have the same charge (0.37). The neutral copper atom (a charge of 0.02) forms the upper corner. The Cu-Ni bonds are equal to 2.411 Å, 2.415 Å, and 2.416 Å. The isomer with Ni on top is higher in energy by 0.70 eV (see Figure S6 for its geometry structure).

The HOMO-LUMO gaps of the Cu_nNi_m - C_3N_4 systems were also narrowed compared to g- C_3N_4 (see Figure 7 for a schematic representation of their electronic structures). While almost all bimetallic systems have similar electronic structures, the band narrowing is the most pronounced in $CuNi_3$ - C_3N_4 .

Similarly, as for the monometallic systems, the binding energies of the metal clusters to the support and metal cluster reorganization energies are calculated (see Table 3).

E_{reor} in [eV] computed for the Cu_mNi_n - C_3N_4 structures at the DFT:PBE/def2-TZVP level.									
System	E _{bin} [eV]	E _{nuc-gas} (Cu) [eV]	E _{nuc-SAC} (Cu) [eV]	E _{nuc-gas} (Ni) [eV]	E _{nuc-SAC} (Ni) [eV]	E _{reor} [eV]			
CuNi-C ₃ N ₄	-2.72	-1.38	0.91	-3.95	0.91	0.02			

-0.33

0.30

-0.96

-0.81

-2.93

Cu₂Ni-C₃N₄

CuNi₂-C₃N₄ Cu₂Ni₂-C₃N₄

Cu₃Ni-C₃N₄

CuNi₃-C₃N₄

-3.48

-3.83

-5.07

-4.27

-5.45

-2.62

-1.99

-3.25

-3.10

-5.23

Table 3. The energetic parameters (E_{bin} , $E_{nuc\text{-}gas}$ (Cu), $E_{nuc\text{-}SAC}$ (Cu), $E_{nuc\text{-}gas}$ (Ni), $E_{nuc\text{-}SAC}$ (Ni), and E_{reor} in [eV] computed for the Cu_mNi_n - C_3N_4 structures at the DFT:PBE/def2-TZVP level.

-5.43

-5.03

-5.66

-5.40

-5.96

-0.57

-0.18

-0.80

-0.54

-1.10

0.08

0.09

0.02

0.52

0.35

All computed E_{bin} values are negative, indicating the favorable interaction between the bimetallic clusters and g- C_3N_4 , thus confirming their stability. The tetrahedral clusters exhibit the most favorable binding energies. This should be attributed to the fact that as many as three atoms form chemical bonds with the support, and the metal atoms form a regular shape with good stability.

Catalysts **2025**, 15, 861

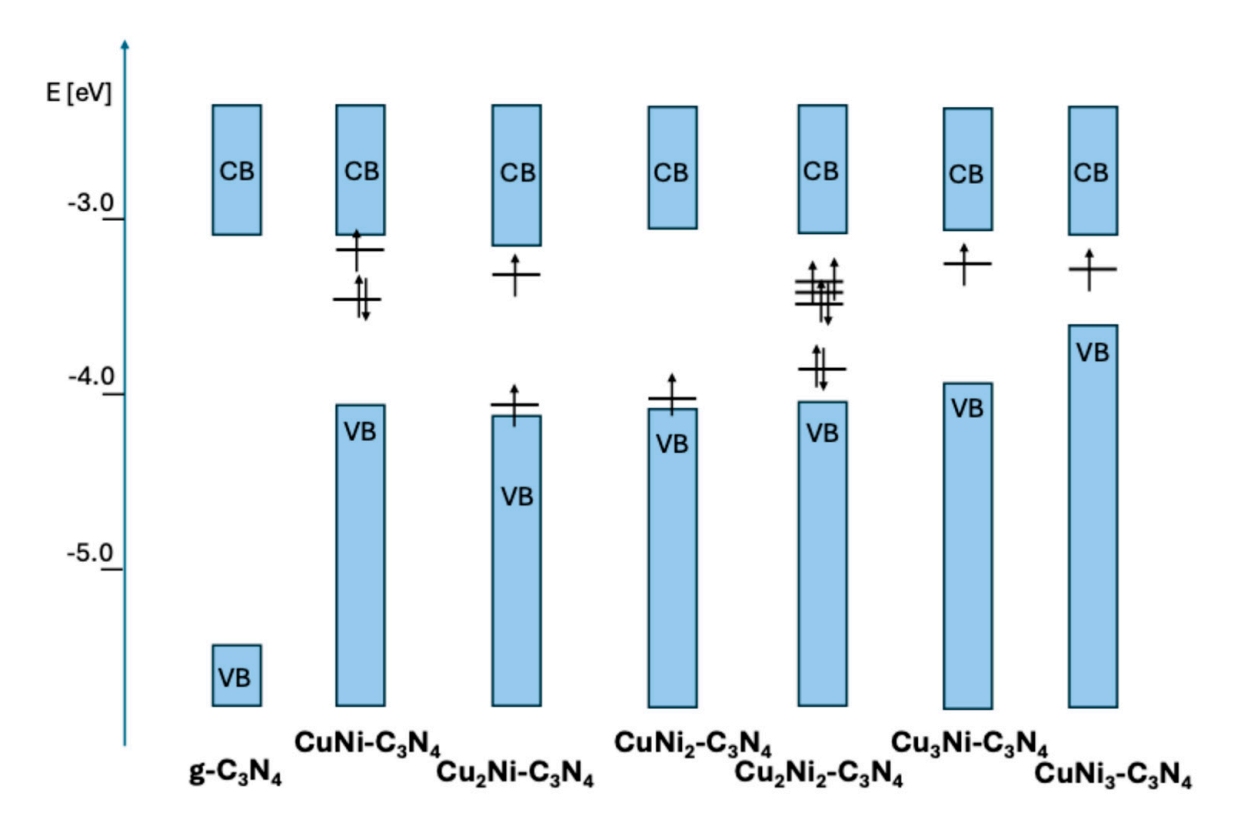


Figure 7. Schematic representation of the electronic structure of the $Cu_nNi_m-C_3N_4$ systems (VB—valence band; CB—conduction band). For the open-shell systems, the diagram represents alpha electrons.

Next, the nucleation energies were calculated. For each of the systems, two scenarios were considered, corresponding to adding either the copper atom from the gas phase/from the g- C_3N_4 anchored site (Cu- C_3N_4) or the nickel atom. Hence, to facilitate the discussion, $E_{nuc\text{-}gas}$ and $E_{nuc\text{-}SAC}$ are additionally indicated by the abbreviation of the element to be added. The binding of the isolated Cu or Ni element to grow the cluster is always favorable (see $E_{nuc\text{-}gas}$ (Cu) and $E_{nuc\text{-}gas}$ (Ni)). The energy values are lower when the extra Ni atom is introduced, which may suggest that it might be easier to form these structures when copper clusters are synthesized first and nickel is then introduced as the second element.

The examination of the values of $E_{nuc\text{-}SAC}$ (Cu) and $E_{nuc\text{-}SAC}$ (Ni) reveals that the formation of the CuNi-C₃N₄ of metal sites already anchored on g-C₃N₄ would not be energetically favorable. Similarly, the overall process of removing Cu from Cu-C₃N₄ and attaching it to Ni₂-C₃N₄ to form CuNi₂-C₃N₄ would require energy input. The remaining nucleation energies are negative, pointing to the possibility of the Cu/Ni migration from their SAC position to grow larger structures.

The computed metal cluster reorganization energies are small for all but the tetrahedral Cu_3Ni and Ni_3Cu ones. The latter have different geometries while in g- C_3N_4 or in the gas phase, giving rise to higher E_{reor} values than computed for the remaining bimetallic structures.

3. Materials and Methods

The present studies were carried out using the Density Functional Theory (DFT) method as implemented in the Turbomole v6.3 suite of programs [34]. The Perdew–Becke–Ernzerhof (PBE) functional was used with the def2-TZVP basis set applied to all atoms. The choice of the functional follows from the previous studies of the C_3N_4 structure, which can be found in previous studies (see, e.g., [21,29], as well as the other SAC-type materials). The

Catalysts **2025**, 15, 861

use of this functional is further justified by earlier studies, which claim that the generalized gradient (GGA) type functionals, PBE in particular, are particularly suited for solid-state materials, including metals [35,36].

For each of the systems under study, different possible multiplicities were considered, but in this manuscript, only those characterized by the lowest total energies are listed. The relative energies of the remaining structures of other multiplicities are listed in Table S1 in the Supplementary Materials.

The applied geometry model of the g- C_3N_4 material involved the basic building unit of the g- C_3N_4 structure comprising three heptazine "triangles" as depicted in Figure 1. To keep the planarity of the support, the carbon atoms at the corners of the g- C_3N_4 model are frozen. All remaining atoms were allowed to move until convergence criteria were met (10^{-6} a.u. for the energy, 10^{-3} for the gradient, and 10^{-6} for the root mean square of the density matrix). It should be noted, however, that the current study has a limitation resulting from the model of g- C_3N_4 used in this study having only one layer. Therefore, the structures in which small metal clusters are located between two layers, forming chemical bonds with nitrogen atoms from two sheets, are not accounted for.

The obtained structures were characterized with a natural population analysis (NPA), which is used to compute charges on the metal atoms.

The following energy parameters were calculated to provide insight into the strength of the metal–support interaction. First, the binding energy (E_{bin}) of the metal atoms to the support is computed as the energy difference between M_n - C_3N_4 (where M=Cu or Ni) and the sum of the energies of M_n and g- C_3N_4 in their fully relaxed geometries:

$$E_{bin} = E(M_n - C_3N_4) - E(M_n) - E(C_3N_4), \tag{1}$$

Next, in order to see the tendency of the metal atoms to aggregate on g- C_3N_4 , the energy needed to add one metal atom to the existing metal– C_3N_4 system from the gas phase ($E_{nuc-gas}$) is as follows:

$$E_{\text{nuc-gas}} = E(M_n - C_3 N_4) - E(M) - E(M_{n-1} - C_3 N_4), \tag{2}$$

and its process of migration from its SAC-like position in M- C_3N_4 (denoted as $E_{nuc\text{-SAC}}$) is represented as follows:

$$E_{\text{nuc-SAC}} = E(M_n - C_3 N_4) + E(C_3 N_4) - E(M - C_3 N_4) - E(M_{n-1} - C_3 N_4), \tag{3}$$

Finally, the energy required to change the geometry of the metal cluster from the optimum in the gas phase to the one in C_3N_4 (E_{reor}) was computed:

$$E_{reor} = E_{Mn-C3N4}(M_n) - E_{gas}(M_n), \tag{4}$$

where $E_{Mn-C3N4}$ (M_n) denotes the energy of the Mn cluster anchored to the g- C_3N_4 and E_{gas} (M_n) energies of the isolated, gas-phase M_n cluster.

4. Conclusions

We have proposed geometry structures of systems in which copper, nickel, and a combination thereof are located in the cavity between the heptazine building units of g- C_3N_4 . Generally, the nickel atoms form shorter bonds with the support than the copper atoms do, which is reflected by the binding energies. We demonstrated that Cu and Ni, when in the form of the isolated single atoms, lie in the plane of the cavity. Once the atoms agglomerate and form small clusters, they tend to bind above the C_3N_4 plane. Based on the observed differences in geometries of the metal clusters, it can be assumed that the

Catalysts **2025**, 15, 861 14 of 17

larger moieties, including metal nanoparticles, will be located above the layers of g- C_3N_4 . This finding has important implications for catalysis. A recent study by Zhang [37] and co-workers demonstrated that the reactivity of the so-called copper single-atom catalysts toward the electroreduction of CO/CO_2 to C_{2+} products should be attributed not only to the Cu_1 sites, but also to the small assemblies of copper atoms. The geometry structures reported in their work resemble the ones described here, with copper pointing above the C_3N_4 plane, facilitating the binding of the reactants and the kinetics of the C-C coupling step of the reaction. The authors underlined the need for at least three Cu atoms in the active site to lower the activation energy for the rate-determining step, not only for Cu-SACs incorporated in graphitic carbon nitride, but also in N-substituted graphene.

Most of the metal sites became oxidized when inserted into the g- C_3N_4 cavity. In particular, this refers to the atoms that form direct bonds with the support. Those that are bound exclusively to the other metal atoms are neutral or slightly negatively charged. The presence of the cations anchored to the support created additional electrophilic sites that can exhibit catalytic properties. The metal sites introduced into the C_3N_4 material can also bind oxygen or water molecules either from solution or from the atmosphere, as demonstrated in [37]. It was shown that under these circumstances, even the single copper atom may be displaced out of the C_3N_4 cavity. Such a behavior may lead to the formation of small clusters of the Cu-O-N phases, whose reactivity and thermodynamic stability have already been studied extensively by Fallberg et al. [38] and Mavrodou et al. [39]. In case of the investigated materials, one can expect the formation of the sub-nanometric Cu_xO_y clusters bound to g- C_3N_4 . CuO/g- C_3N_4 hybrids have been recently reported to be efficient electrode materials [40] and active catalysts for reduction reactions [41,42].

An analysis of the electronic structures of the investigated systems indicates that the HOMO-LUMO gap is narrowing. Additionally, the in-band electronic states appeared due to the incorporation of metal atoms into the g- C_3N_4 support. The observed changes justify why the materials are frequently used for photocatalysis.

All investigated single-metal atoms and their small clusters exhibit negative binding energies, meaning that the $Cu/Ni-C_3N_4$ composites should be stable, and the metal species will not easily leach from the support. Furthermore, the investigated clusters have the potential to grow once the additional Cu or Ni atoms are introduced to the system, as demonstrated by the negative nucleation energies ($E_{nuc-gas}$). However, the energy needed to migrate the single atom from its SAC-like position ($M-C_3N_4$; M=Cu, Ni) is positive in the selected cases: $Cu_2-C_3N_4$, $Ni_2-C_3N_4$, $Ni_3-C_3N_4$, and $CuNi-C_3N_4$. This results from the higher stability of the single-copper or -nickel sites than of these structures.

Finally, the stabilities of the tetrahedral clusters are the largest. This shows that the cavity formed between the heptazine "triangles" in g- C_3N_4 and the type of anchoring atoms are the right fit for this size of metal species, explaining the increasing number of articles that report on the claims of tetrahedral M_4 clusters binding to g- C_3N_4 and their activities in various catalytic reactions [12,13].

Supplementary Materials: The following supporting information can be downloaded at: https://www.mdpi.com/article/10.3390/catal15090861/s1: Table S1: Relative DFT:PBE/def2-TZVP energies (in Hartree) of the structures with different spin multiplicities calculated in the current study. In the main manuscript, only structures of the lowest total energies are discussed. Figure S1: The DFT:PBE/def2-TZVP structure of the Cu₄-C₃N₄ isomer found in the current studies. The most characteristic bond lengths are given in Ångstroms. Atom color coding: Cu—pink; Ni—green; C—gray; N—blue; H—white. Figure S2: The DFT:PBE/def2-TZVP structures of the Cu₂Ni-C₃N₄ isomers found in the current studies. The most characteristic bond lengths are given in Ångstroms. Atom color coding: Cu—pink; Ni—green; C—gray; N—blue; H—white. Figure S3: The DFT:PBE/def2-TZVP structure of the CuNi₂-C₃N₄ isomer found in the current studies. The most characteristic bond lengths

Catalysts 2025, 15, 861 15 of 17

are given in Ångstroms. Atom color coding: Cu—pink; Ni—green; C—gray; N—blue; H—white. Figure S4: The DFT:PBE/def2-TZVP structure of the $Cu_2Ni_2-C_3N_4$ isomer found in the current studies. The most characteristic bond lengths are given in Ångstroms. Atom color coding: Cu—pink; Ni—green; C—gray; N—blue; H—white. Figure S5: The DFT:PBE/def2-TZVP structures of the $Cu_3Ni-C_3N_4$ isomer found in the current studies. The most characteristic bond lengths are given in Ångstroms. Atom color coding: Cu—pink; Ni—green; C—gray; N—blue; H—white. Figure S6: The DFT:PBE/def2-TZVP structures of the CuNi $_3$ -C $_3N_4$ isomer found in the current studies: The most characteristic bond lengths are given in Ångstroms. Atom color coding: Cu—pink; Ni—green; C—gray; N—blue; H—white.

Author Contributions: Conceptualization and methodology, A.D.-M., P.S., and D.R.-Z.; investigation, A.D.-M., P.S., and D.R.-Z.; writing—original draft preparation, D.R.-Z.; writing—review and editing, D.R.-Z.; funding acquisition, P.S. All authors have read and agreed to the published version of the manuscript.

Funding: This research was funded by the National Science Centre (Poland), POLONEZ BIS 3 project reg. no. 2022/47/P/ST4/03412, and the European Union's Horizon 2020 research and innovation program and Marie Skłodowska-Curie Actions, grant agreement no. 945339.

Data Availability Statement: Data are available in a publicly accessible repository: https://repod.icm.edu.pl (accessed on 2 September 2025).

Conflicts of Interest: The authors declare no conflicts of interest.

Abbreviations

The following abbreviations are used in this manuscript:

g-C₃N₄ Graphitic Carbon Nitride DFT Density Functional Theory NPA Natural Population Analysis SAC Single-Atom Catalyst

References

- 1. Wang, Y.; Mao, J.; Meng, X.; Yu, L.; Deng, D.; Bao, X. Catalysis with Two-Dimensional Materials Confining Single Atoms: Concept, Design, and Applications. *Chem. Rev.* **2019**, *119*, 1806–1854. [CrossRef] [PubMed]
- 2. Nashim, A.; Parida, K. A Glimpse on the plethora of applications of prodigious material MXene. *Sustain. Mater. Technol.* **2022**, 32, e00439. [CrossRef]
- 3. Alam, M.W.; Allag, N.; Naveed-Ur-Rehman, M.; Islam Bhat, S. Graphene-Based Catalysts: Emerging Applications and Potential Impact. *Chem. Rec.* **2024**, 24, e202400096. [CrossRef]
- 4. Yruela-Garrido, M.; Campos-Castellanos, E.; Morales, M.V.; Rodríguez-Ramos, I.; Guerrero-Ruiz, A. Boron Nitride-Supported Metal Catalysts for the Synthesis and Decomposition of Ammonia and Formic Acid. *Nanomaterials* **2025**, *15*, 212. [CrossRef]
- 5. Li, H.; Cheng, B.; Xu, J.; Yu, J.; Cao, S. Crystalline carbon nitrides for photocatalysis. EES Catal. 2024, 2, 411–447. [CrossRef]
- 6. Lu, Q.; Eid, K.; Li, W.; Abdullah, A.M.; Xu, G.; Varma, R.S. Engineering graphitic carbon nitride (g-C₃N₄) for catalytic reduction of CO₂ to fuels and chemicals: Strategy and mechanism. *Green Chem.* **2021**, *23*, 5394–5428. [CrossRef]
- 7. Yang, X.-F.; Wang, A.; Qiao, B.; Li, J.; Liu, J.; Zhang, T. Single-Atom Catalysts: A New Frontier in Heterogeneous Catalysis. *Acc. Chem. Res.* **2013**, *46*, 1740–1748. [CrossRef]
- 8. Kaiser, S.K.; Chen, Z.; Faust Akl, D.; Mitchell, S.; Pérez-Ramírez, J. Single-Atom Catalysts across the Periodic Table. *Chem. Rev.* **2020**, *120*, 11703–11809. [CrossRef]
- 9. Liu, L.; Corma, A. Metal Catalysts for Heterogeneous Catalysis: From Single Atoms to Nanoclusters and Nanoparticles. *Chem. Rev.* **2018**, *118*, 4981–5079. [CrossRef]
- 10. Zhou, Y.; Gao, G.; Li, Y.; Chu, W.; Wang, L.-W. Transition-metal single atoms in nitrogen-doped graphenes as efficient active centers for water splitting: A theoretical study. *Phys. Chem. Chem. Phys.* **2019**, *21*, 3024–3032. [CrossRef]
- 11. Zhou, P.; Lv, F.; Li, N.; Zhang, Y.; Mu, Z.; Tang, Y.; Lai, J.; Chao, Y.; Luo, M.; Lin, F.; et al. Strengthening reactive metal-support interaction to stabilize high-density Pt single atoms on electron-deficient g-C₃N₄ for boosting photocatalytic H₂ production. *Nano Energy* **2019**, *56*, 127–137. [CrossRef]

Catalysts **2025**, 15, 861 16 of 17

12. Zhang, S.; Feng, H.; Tang, R.; Li, H.; Wu, Y. Mechanism of transition-metal-cluster-anchored g-C₃N₄ for the electrochemical catalytic hydrogenation of carbon dioxide to C1 products. *Comput. Theor. Chem.* **2025**, *1244*, 115076. [CrossRef]

- 13. Zhang, S.; Feng, H.; Li, C.; Cao, X.; Li, H.; Wu, Y. The reduction mechanism of C1 product from carbon dioxide catalyzed by Ni-doped g-C₃N₄. *Mol. Catal.* **2024**, 559, 114064. [CrossRef]
- 14. Zhang, Y.; Li, S.; Sun, C.; Cao, X.; Wang, X.; Yao, J. Defective g-C₃N₄ supported Ru₃ single-cluster catalyst for ammonia synthesis through parallel reaction pathways. *Nano Res.* **2023**, *16*, 3580–3587. [CrossRef]
- 15. An, S.; Zhang, G.; Wang, T.; Zhang, W.; Li, K.; Song, C.; Miller, J.T.; Miao, S.; Wang, J.; Guo, X. High-Density Ultra-small Clusters and Single-Atom Fe Sites Embedded in Graphitic Carbon Nitride (g-C₃N₄) for Highly Efficient Catalytic Advanced Oxidation Processes. *ACS Nano* 2018, 12, 9441–9450. [CrossRef]
- 16. Dziadyk, E.; Trawczyński, J.; Szyja, B.M. The pathways of the CO₂ hydrogenation by NiCu/ZnO from DFT molecular dynamics simulations. *J. Mol. Graph. Model.* **2020**, *100*, 107677. [CrossRef]
- 17. Wang, C.; Lv, P.; Xue, D.; Cai, Y.; Yan, X.; Xu, L.; Fang, J.; Yang, Y. Zero-Dimensional/Two-Dimensional Au₂₅(Cys)₁₈ Nanoclusters/g-C₃N₄ Nanosheets Composites for Enhanced Photocatalytic Hydrogen Production under Visible Light. *ACS Sustain. Chem. Eng.* **2018**, *6*, 8447–8457. [CrossRef]
- 18. Wang, Z.; Fan, J.; Cheng, B.; Yu, J.; Xu, J. Nickel-based cocatalysts for photocatalysis: Hydrogen evolution, overall water splitting and CO₂ reduction. *Mater. Today Phys.* **2020**, *15*, 100279. [CrossRef]
- 19. Wu, Q.; Wei, W.; Lv, X.; Wang, Y.; Huang, B.; Dai, Y. Cu@g-C₃N₄: An Efficient Single-Atom Electrocatalyst for NO Electrochemical Reduction with Suppressed Hydrogen Evolution. *J. Phys. Chem. C* **2019**, *123*, 31043–31049. [CrossRef]
- 20. Yang, T.; Mao, X.; Zhang, Y.; Wu, X.; Wang, L.; Chu, M.; Pao, C.-W.; Yang, S.; Xu, Y.; Huang, X. Coordination tailoring of Cu single sites on C₃N₄ realizes selective CO₂ hydrogenation at low temperature. *Nat. Commun.* **2021**, *12*, 6022. [CrossRef]
- 21. Allasia, N.; Xu, S.; Jafri, S.F.; Borfecchia, E.; Cipriano, L.A.; Terraneo, G.; Tosoni, S.; Mino, L.; Di Liberto, G.; Pacchioni, G.; et al. Resolving the Nanostructure of Carbon Nitride-Supported Single-Atom Catalysts. *Small* **2025**, *21*, e2408286. [CrossRef]
- 22. Panigrahi, P.; Kumar, A.; Karton, A.; Ahuja, R.; Hussain, T. Remarkable improvement in hydrogen storage capacities of two-dimensional carbon nitride (g-C₃N₄) nanosheets under selected transition metal doping. *Int. J. Hydrogen Energy* **2020**, 45, 3035–3045. [CrossRef]
- 23. Sun, Y.; Wang, S.; Jia, J.; Liu, Y.; Cai, Q.; Zhao, J. Supported Cu₃ clusters on graphitic carbon nitride as an efficient catalyst for CO electroreduction to propene. *J. Mater. Chem. A* **2022**, *10*, 14460–14469. [CrossRef]
- 24. Zhang, Y.; Sun, H.; Chen, C. New template for metal decoration and hydrogen adsorption on graphene-like C₃N₄. *Phys. Lett. A* **2009**, *373*, 2778–2781. [CrossRef]
- 25. Stottko, R.; Dziadyk-Stopyra, E.; Szyja, B.M. Can Machine Learning Predict the Reaction Paths in Catalytic CO₂ Reduction on Small Cu/Ni Clusters? *Catalysts* **2023**, *13*, 1470. [CrossRef]
- 26. Zhao, X.; Wang, L.; Pei, Y. Single Metal Atom Catalyst Supported on g-C₃N₄ for Formic Acid Dehydrogenation: A Combining Density Functional Theory and Machine Learning Study. *J. Phys. Chem. C* **2021**, 125, 22513–22521. [CrossRef]
- 27. Laboratory, L.B.N. Materials Project Database. Available online: https://next-gen.materialsproject.org/materials/mp-30 (accessed on 29 July 2025).
- 28. Yang, L.-M.; Frauenheim, T.; Ganz, E. Properties of the Free-Standing Two-Dimensional Copper Monolayer. *J. Nanomater.* **2016**, 8429510. [CrossRef]
- 29. Li, H.; Zhang, Z.; Liu, Y.; Cen, W.; Luo, X. Functional Group Effects on the HOMO–LUMO Gap of g-C₃N₄. *Nanomaterials* **2018**, *8*, 589. [CrossRef] [PubMed]
- 30. Li, W. Influence of electronic structures of doped TiO₂ on their photocatalysis. *Phys. Status Solidi (RRL)-Rapid Res. Lett.* **2015**, 9, 10–27. [CrossRef]
- 31. Li, C.-G.; Shen, Z.-G.; Hu, Y.-F.; Tang, Y.-N.; Chen, W.-G.; Ren, B.-Z. Insights into the structures and electronic properties of Cu_{n+1}^{μ} and $Cu_nS^{\mu}(n=1-12; \mu=0, \pm 1)$ clusters. *Sci. Rep.* **2017**, *7*, 1345.
- 32. Güven, M.H.; Eryürek, M. Dynamical and Structural Properties of the Ni₄ Cluster. *Phys. Status Solidi B* **1999**, 213, 283–295. [CrossRef]
- Grigoryan, V.G.; Springborg, M. Structural and energetic properties of nickel clusters: 2 ≤ N ≤ 150. Phys. Rev. B 2004, 70, 205415.
 [CrossRef]
- 34. TURBOMOLE V6.3 2011, a.d.o.U.o.K.a.F.K.G., 1989-2007, and s.a.f.h.w.t.c. TURBOMOLE GmbH, *TURBOMOLE V6.3 2011, A Development of University of Karlsruhe and Forschungszentrum Karlsruhe GmbH*, 1989-2007, TURBOMOLE GmbH, Since 2007. Available online: http://www.turbomole.com (accessed on 7 February 2011).
- 35. Gao, W.; Abtew, T.A.; Cai, T.; Sun, Y.-Y.; Zhang, S.; Zhang, P. On the applicability of hybrid functionals for predicting fundamental properties of metals. *Solid State Commun.* **2016**, 234–235, 10–13. [CrossRef]
- 36. Haas, P.; Tran, F.; Blaha, P.; Schwarz, K.; Laskowski, R. Insight into the performance of GGA functionals for solid-state calculations. *Phys. Rev. B* **2009**, *80*, 195109. [CrossRef]

Catalysts 2025, 15, 861 17 of 17

37. Zhang, J.; Wang, Y.; Li, Y. Not One, Not Two, But at Least Three: Activity Origin of Copper Single-Atom Catalysts toward CO₂/CO Electroreduction to C₂₊ Products. *J. Am. Chem. Soc.* **2024**, *146*, 14954–14958. [CrossRef]

- 38. Fallberg, A.; Ottosson, M.; Carlsson, J.-O. Phase stability and oxygen doping in the Cu–N–O system. *J. Cryst. Growth* **2010**, *312*, 1779–1784. [CrossRef]
- 39. Mavridou, K.; Zervos, M.; Pinakidou, F.; Brzhezinskaya, M.; Katsikini, M. Oxidation of Cu₃N thin films obtained from Cu annealed under NH₃:O₂ flow: A Raman and N-K-edge NEXAFS study. *J. Alloys Compd.* **2022**, 914, 165293. [CrossRef]
- 40. Subhash, K.G.; Benoy, M.D.; Duraimurugan, J.; Siranjeevi, R.; Prabhu, S. Synthesis, and characterization of CuO/g-C₃N₄ nanocomposites for high performances supercapacitor application. *Mater. Lett.* **2023**, *330*, 133288. [CrossRef]
- 41. Sung, C.-L.; Wang, R.-H.; Shih, Y.-C.; Wu, Z.-Y.; Alvarado, S.R.; Chang, Y.-H.; Lin, C.-C. g-C₃N₄ Nanosheet Supported CuO Nanocomposites for the Electrochemical Carbon Dioxide Reduction Reaction. *ACS Omega* **2023**, *8*, 7368–7377. [CrossRef]
- 42. Suresh, R.; Karthikeyan, N.S.; Gnanasekaran, L.; Rajendran, S.; Soto-Moscoso, M. Facile synthesis of CuO/g-C₃N₄ nanolayer composites with superior catalytic reductive degradation behavior. *Chemosphere* **2023**, *315*, 137711. [CrossRef]

Disclaimer/Publisher's Note: The statements, opinions and data contained in all publications are solely those of the individual author(s) and contributor(s) and not of MDPI and/or the editor(s). MDPI and/or the editor(s) disclaim responsibility for any injury to people or property resulting from any ideas, methods, instructions or products referred to in the content.